Journal of The Electrochemical Society, **153** (12) G1025-G1031 (2006)
0013-4651/2006/153(12)/G1025/7/$20.00 © The Electrochemical Society

Iron Thin Films from $Fe(CO)_5$ and $FeCp_2/H_2O$ under Atmospheric Pressure

F. Senocq,[z] F.-D. Duminica, F. Maury,[*] T. Delsol, and C. Vahlas[*]

Centre Interuniversitaire de Recherche et d'Ingénierie des Matériaux CNRS/INPT, ENSIACET, 31077 Toulouse Cedex 4, France

Iron layers were first obtained from iron pentacarbonyl in metallorganic chemical vapor deposition (MOCVD) process under atmospheric pressure, in the temperature range 473–773 K, in a vertical cold wall reactor. Films of good purity were obtained with or without hydrogen as co-reactant, no chemical additives being used. The experiments showed that the velocity of the gas stream and, to a lower extent, the precursor molar fraction are the key parameters to be controlled, in order to monitor film growth rate and purity. In a second step, Fe thin layers were obtained by atmospheric pressure MOCVD starting from the reactive gas mixture $FeCp_2$ and H_2O in the temperature range 973–1073 K. A thermochemical simulation of the Fe-C-H-O system allowed optimum processing conditions to be approached. X-ray diffraction and microprobe analysis showed that the highest iron content in the layer was obtained for $H_2O/FeCp_2$ ratios between 4 and 6. Film growth occurs in two steps: the initial formation of a black, powdered, and porous layer that becomes densified as a result of the grain growth on increasing the deposition time in order to form compact gray metal films. This two-step mechanism was confirmed by kinetic and in situ IR pyrometric observations.
 [DOI: 10.1149/1.2352050]

Manuscript submitted April 7, 2006; revised manuscript received July 18, 2006. Available electronically October 10, 2006.

Our aim was to study chemical vapor deposition of iron thin films for metallurgical applications. Indeed, continuous deposition, or strip coating, can be highly relevant as a form of surface treatment in metallurgy. A suitable process needs at least to fulfill three requirements: (*i*) deposition at low temperature to avoid dimensional and structural changes of the steel substrate, (*ii*) a high growth rate to compensate for the speed of the strip, and (*iii*) operation at atmospheric pressure, which is highly preferable for technical and economical reasons. The use of metallorganic compounds as molecular precursors satisfies the first requirement. For the other two, new processes and optimization of metallorganic chemical vapor deposition (MOCVD) processes already reported in the literature are necessary.

Compared to other metals, few open scientific publications refer to thermal CVD of iron, even though many are devoted to the preparation of iron oxides, sulfides, or silicides. Little attention seems to have been paid to the optimization of the growth rate, which is nevertheless necessary for a continuous deposition process. Moreover, a limited number of molecular precursors have been studied, namely, $Fe(CP)_2$,[1] $Fe(CO)_5$,[2-7] $Fe_2Cp_2(CO)_4$,[8] $Fe[N(SiMe_3)_2]_3$,[9] and $Fe(COT)(CO)_3$.[10] Most of the processes reported operate under low pressure, and rare are those working under atmospheric pressure. Highly textured [011] α iron films (bcc) are reported to have been prepared from ferrocene[1] under 10^5 Pa of H_2, in the temperature range 673–1173 K, but with selective deposition, and no growth rate is given. In the case of iron pentacarbonyl, high growth rates are reported, up to 2 μm/h,[5]at moderate temperature and under atmospheric pressure of hydrogen. However, rising temperature lowers the growth rate,[5,6] but the use of additives like 1,2,3,4,5-pentamethyl-cyclopentadiene in the vapor phase softens this trend,[6]

In addition to the open literature, patents refer mainly to two families of precursors: (*i*) $Fe(CO)_5$ and its derivatives and (*ii*) $Fe(CP)_2$ and related compounds. As $Fe(CO)_2$ vapor pressure is too high to easily control the low mole fractions required for microelectronic applications, Long[11] chose $Fe(CO)_3(C_4H_6)$ and $Fe(CO)_3(C_8H_8)$, for Fe doping of InP layers, between 923 and 973 K. He found that the butadiene derivative gave more promising results than $Fe(CP)_2$, and attributed this to its low decomposition temperature [$\leq$523 K,[12] to be compared to $\geq$723 K [13] for $Fe(Cp)_2$]. Owing to the high vapor pressure of $Fe(CO)_5$, McCormick[14,15]suggested the use of the derivatives $Fe(CO)_4L$, where L is either a phosphine, a phosphite, or an amine group, or the family $[Fe(CO)_3]_2(C_4R_4)$, where each R can be H, a halide, OH, an alkyl, or an aryl moiety. Each of the molecules proposed can be prepared using $Fe(CO)_2$ as a starting material. For example, $Fe(CO)_4(NMe_3)$, $Fe(CO)_4[P(OMe)_3]$, and $Fe_2(CO)_6(C_4H_4)$ were used, without carrier gas, under dynamic vacuum (0.13–1.33 Pa) to prepare smooth and shiny films with a metallic appearance, but containing high amounts of hetero-atoms (as high as 34 atom % C, or 23 atom % P). This is evidence that a clean decomposition of these metallorganic complexes is not observed. Moreover, the toxicity of $Fe(CO)_5$ and its derivatives limits their use, at least in large-scale processes. To bypass this shortcoming, ferrocene has been used, i.e., under oxidative atmosphere, to obtain thin oxide layers, as patented by Kane and Schweizer in 1975.[16] In other conditions, Mukaida et al. patented the use of $FeCp_2$ for the preparation of β-$FeSi_2$.[17] In both cases, the toxicity of $Fe(CO)_5$ was put forward to account for not using this molecule. The alkyl-cyclopentadienyl derivatives [general formula: $(R^1C_5H_4)_{2-p}M(R^2)_p$, where R^1 is alkyl, R^2 is H, F, or alkyl, and M is a metal, which can be Fe] have been proposed[18] to obtain oxide layers under oxidative atmosphere. The precursors belonging to this family are claimed to have vapor pressures over 13 Pa at 373 K, but no specific example of iron oxide deposition is given. Besides these two families, iron acetylacetonate has been proposed for magnetic coating of iron oxide spinels,[19,20] with or without O_2, but it was established that pure iron films were out of reach with this precursor. More recently,[21] Choi et al. proposed another kind of organometallic compounds [of the general formula $R^1_m M(PR^2_3)_x$, with R^1 = H, D, H_2, D_2, alkyl; R^2 = alkyl, aryl; and M = VIIB and VIIIB group metal] to obtain high-purity metallic films or powders.

A promising class of organometallic precursors for deposition of transition metals is the metallocenes; among them, ferrocene ($FeCp_2$) was previously used.[22,23] $FeCp_2$ is easy to synthesize and purify, stable in air, and nontoxic. It has a relatively low vapor pressure (ca. 1.3 Pa at 303 K), and the good thermal stability of this compound allows heating at sufficiently high temperatures to significantly increase its vapor pressure.[24] Such thermal stability imposes relatively high pyrolysis temperatures (up to 773 K) at which an autocatalytic decomposition reaction occurs in the gas phase and leads to the formation of a black powder, which primarily consists of iron contaminated by graphitic carbon and traces of Fe_3C (cementite). According to the literature, reasonably pure Fe films have been deposited by low-pressure CVD to limit gas-phase nucleation, but it is very difficult to obtain such films under atmospheric pressure using inert carrier gas. Elihn et al. employed oxygen to decrease the carbon contamination under atmospheric pressure with a gas mix-

* Electrochemical Society Active Member.
[z] E-mail: Francois.Senocq@ensiacet.fr

Table I. Typical MOCVD conditions for the growth of Fe layers under atmospheric pressure starting from different $H_2O/FeCp_2$ molar ratios.

No. run	1	2	3
Growth temperature (K)	973	1023	1073
Carrier gas flow rate (N_2, sccm)	4950	4900–5100	4950
Total gas flow rate (sccm)	5500	5500	5500
$H_2O/FeCp_2$ molar ratio	5.5	1.9–6.3	5.5
Co-reagent H_2O (sccm)	82	31–82	82
$FeCp_2$ sublimation temperature (K)	373	368–375	373
$FeCp_2$ mole fraction	2.7×10^{-3}	$(2.3–3.5) \times 10^{-3}$	2.7×10^{-3}
Deposition time (min)	15	10–24	15

ture containing 99–99.5% argon and 0.5–1% of oxygen.[25] They observed a decrease of carbon in the nanoparticles thus formed, but they also raised the question of the presence of Fe_2O_3, in addition to iron.[25,26]

The selection of the molecular precursor is a key point for the development of MOCVD processes. The choice strongly depends on the application and the constraints of the deposition process.[27] For metallurgical coating applications, continuous deposition of pure Fe films is advantageous as they could be used, for instance, in strip coating. In this objective, high growth rates and atmospheric pressures are significant requirements for the CVD process. In this paper, we report an investigation of MOCVD of Fe films under atmospheric pressure using $Fe(CO)_5$ as an iron source under various conditions, and from the reactive gas mixture $FeCp_2$ and H_2O in the temperature range 973-1073 K. Preliminary results were recently reported at an ECS meeting, using $Fe(CO)_5$ [28] and $FeCp_2/H_2O$.[29] Here, the experimental details are reported and the results discussed in relation with data from the literature. Thermodynamic calculations were carried out to predict and optimize the growth conditions from this gas mixture and the growth mechanism is discussed.

Experimental

The CVD experiments were conducted in a vertical tubular cold-wall reactor, 46 mm i.d., under atmospheric pressure, the substrates [Si(111) wafers or stainless steel coupons] being placed on a stainless steel sample holder (32 mm in diameter, 40 mm high) heated by HF induction. Nitrogen was used as carrier gas, and either hydrogen or nitrogen were used as dilution gas. The gas flows were monitored with mass-flow meters.

$Fe(CO)_2$ and $FeCp_2$ mole fractions were controlled by monitoring the temperature of the thermostated saturators and were determined from precursor mass loss. The same procedure was followed for the water vapor mole fraction in experiments with $FeCp_2$. In both cases, N_2 was the carrier gas of the precursors, and, with $FeCp_2$, the total flow rate was 5500 standard cubic centimeters per minute (sccm) to reach laminar flow above the surface of the substrates. Typical MOCVD conditions for the growth of Fe layers under atmospheric pressure starting from different $H_2O/FeCp_2$ molar ratios are presented in Table I, and those starting from $Fe(CO)_5$ in Table II.

The microstructure of the films obtained was studied by X-ray diffraction (Cu Kα, diffracted beam monochromator). Scanning electron microscopy (SEM) was used to investigate surface morphology, and film thicknesses were determined through observations of cross sections and from the mass gain of the samples. The film composition was analyzed by electron probe microanalysis (EPMA).

Results and Discussion

$Fe(CO)_5$.— Using $Fe(CO)_5$ without additive, incorporation of carbon or oxygen from the carbonyl ligands in the layer could be expected, so the first experiments were carried out under hydrogen. With a carrier gas flow rate of 30 sccm of N_2 and 200 sccm of H_2, and with precursor molar fractions of 2×10^{-3} or 6.75×10^{-3}, no deposition occurs for a substrate temperature of 443 K, this pyrolysis temperature likely being too low in the gas flow conditions chosen. At 473 K, thick films were formed at growth rates as high as 50 μm/h, but with intense spallation, even during growth. The "self-destruction" of the film was attributed to too high a growth rate, which causes too much strain in the film and poor adhesion to the substrate. From 523 to 673 K, adhesive shiny gray metallic films were obtained.

XRD analysis (Fig. 1) shows that these films are made of iron, with Fe_3C (cementite) as secondary phase (no crystallized graphitic carbon was detected). A slight texturation along the (110) axis of iron was observed (texturation coefficient ≈2). Application of the Scherrer law gave a mean crystallite size of ca. 10 nm in the temperature range 473–573 K, rising to ca. 25 nm at 623 K. As EPMA analysis (see below) showed that the carbon content was steady (1–2 atom %) in the temperature range 523–623 K, the difference in the apparent Fe/Fe_3C ratio in X-ray diagrams can be attributed to a better crystallization of iron at higher temperatures.

The SEM observations show smooth and homogeneous surface morphologies, while analysis of cross sections reveals an evolution of the morphology with the temperature: porous with columnar growth until 553 K, and lamellar beyond this temperature (Fig. 2).

The composition of the films was investigated with EPMA analyses: at 473 K, iron was 90 atom % as carbon was up to 10%. The large quantities of carbon may come from the deposition temperature being too low, which could lead to incomplete decomposition of the precursor, and its subsequent incorporation into the film, owing to the high growth rate. In the temperature range 523–623 K, the iron rose to ca. 98 atom %, and carbon to ca. 1–2%. The oxygen content was very low, below the detection limits. At 673 K, the iron

Table II. Growth rates and composition (EPMA) of films deposited under atmospheric pressure starting from $Fe(CO)_5$ for various experimental conditions.

						EPMA	
Run	K	Flow rate (sccm)	Mole fraction	V gas (cm/s)	Growth rate (μm/h)	Fe	C
E6	673	$200H_2+30N_2$	6.7×10^{-3}	0.25	0.3	90	6
D2	673	1147 (N_2)	1.0×10^{-2}	1.16	1.6	89	11
D12	673	2320 (N_2)	2.2×10^{-3}	2.33	2.0	95	5
D26	673	10,000 (N_2)	7.0×10^{-3}	10.06	4.5	92	8
D14	773	5,000 (N_2)	1.0×10^{-3}	5.02	0.16	94	6
D27	773	10,000 (N_2)	7.0×10^{-3}	10.06	0.6	92	8

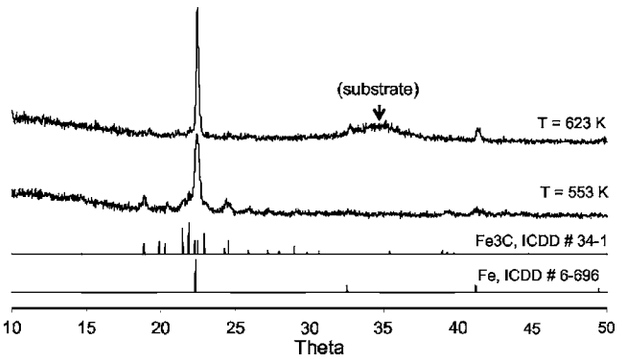

Figure 1. XRD diagrams (grazing incidence 2°) of iron films deposited from $Fe(CO)_5$ and H_2 on silicon wafer.

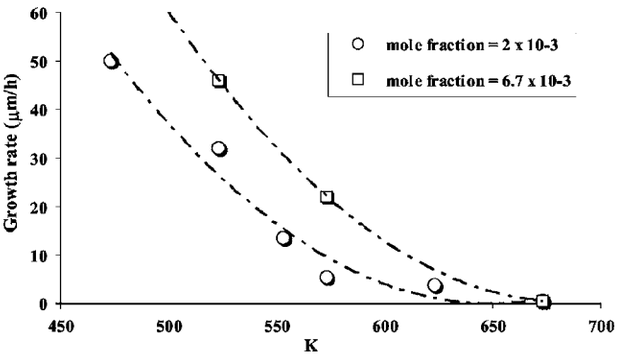

Figure 3. Growth rates vs deposition temperature, for different molar fractions, in the temperature range 473–673 K, 230 sccm total flow rate (30 sccm N_2 + 200 sccm H_2). The dotted curves are a guide for the eyes.

content dropped to 90%, as C and O rose to ca. 5% each. The lower film purity can be correlated to the homogeneous decomposition of $Fe(CO)_5$ observed in the gas phase from ca. 623 K.

The growth rate was estimated by SEM observation of cross sections of samples, or on scales for the thickest deposits where they had become detached from the substrate (Fig. 2b). A decrease in growth rate with increasing deposition temperature was observed (Fig. 3), the upper limit being apparently 673 K, for which the deposition rate was very low ($\leq$0.3 μm/h for a molar fraction of 2×10^{-3} or 6.75×10^{-3}). This behavior has already been reported for $Fe(CO)_5$[5,6] and for $Ni(CO)_4$,[5,30] and is imputed to (*i*) homogeneous gas-phase reactions of the reactant and (*ii*) surface reactions of CO released by deposition and decomposition reactions to re-form volatile iron species.

An increase of growth rate with molar fraction was observed, but it did not allow deposition beyond 673 K. Experiments done at higher temperatures, and with low flow rates, show intense homogeneous decomposition of the precursor, leading to black soot in the reactor and thin, black, nonadhesive crumpled films. As the thermal limitation of the deposition reaction could be attributed to (*i*) homogeneous decomposition reactions and (*ii*) surface side reactions due to poor byproduct elimination, and also to far too long residence times of different chemical species in the reaction zone, it seemed promising to shorten the residence time by increasing the total flow rate. This was done by raising the overall flow rate (up to 10,000 sccm). As it is possible to get pure metal films from metal carbonyls such as $Ni(CO)_4$ without using a reductive atmosphere[30] and in order to avoid the dangers of large hydrogen output, pure nitrogen was used both as dilution and carrier gas.

The first noticeable effect of the increase of flow rate was to drop the homogeneous decomposition of $Fe(CO)_5$ previously observed (i.e., run E6). It was thus possible to prepare iron films in such conditions at 673 K, with an overall gas flow rate of 1147 sccm. As for the films prepared at low temperature under H_2, XRD diagrams (Fig. 4) show the diffraction lines of iron. The other lines were attributed to iron oxide Fe_2O_3, no graphitic carbon or iron carbide being detected. Similar diagrams were obtained from samples prepared at 773 K with a higher flow rate, although a slight increase of iron oxide amount was observed. The SEM observations of the surfaces and of the cross sections of samples grown at 673 and 773 K showed smooth and homogeneous layers, with regular thickness, and equi-axial grain growth.

The growth rates increased with the total flow rate (Table II), and then with the gas velocity. For similar mole fractions, the growth rate was 0.3 μm/h at 673 K with 230 sccm flow rate (run E6), and 4.5 μm/h with 10,000 sccm (run D26). Nevertheless, as observed before, the growth rate dropped when the temperature was increased from 673 K (4.5 μm/h, run D26) to 773 K (0.6 μm/h, run D27), keeping constant the flow rate and mole fraction. As homogeneous decomposition is nearly completely avoided, the reverse reaction that gives volatile iron species from iron film and releases CO seemed to dominate. Moreover, the higher the $Fe(CO)_5$ mole fraction, the higher the incorporation of carbon in the film, which prevents the growth of pure metal layers at high mole fractions.

$FeCp_2$.— When $FeCp_2$ was used without any additive, a self-catalyzed decomposition reaction occurred in the gas phase over 813 K leading to black soot and a black nonadhesive deposit mainly composed of pulverulent graphitic carbon, untextured iron, and some cementite Fe_3C. Shortening the residence time by increasing the total flow rate as previously done for $Fe(CO)_5$ did not improve the film quality. Below 813 K, the growth was very slow, due to a low pyrolysis rate.

To allow the use of $FeCp_2$, a well-chosen additive is therefore necessary. As H_2 is not recommended in large-scale applications for security reasons, the effect of water vapor, which is cheap, nontoxic, and risk-free, was investigated. Along with the experiments, a thermodynamic simulation of the $FeCp_2/H_2O$ system was performed.

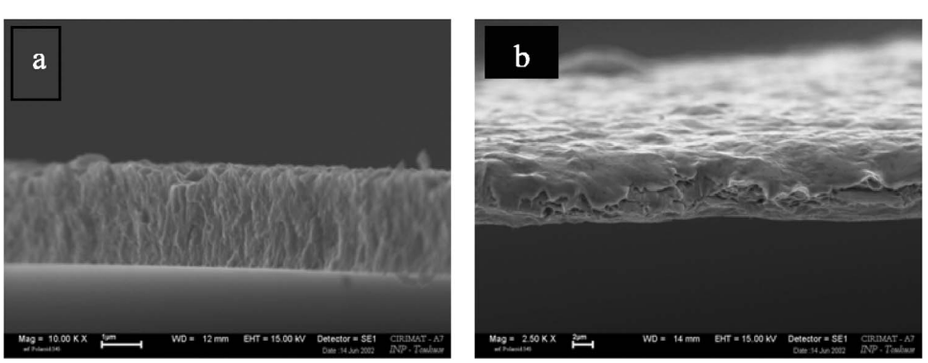

Figure 2. SEM cross section of iron films on silicon wafer obtained at 553 K (a, left) and 623 K (b, right) from $Fe(CO)_5$ and H_2. (b) shows a film flake detached from substrate. The white bars below the pictures represent 1 μm (left) and 2 μm (right).

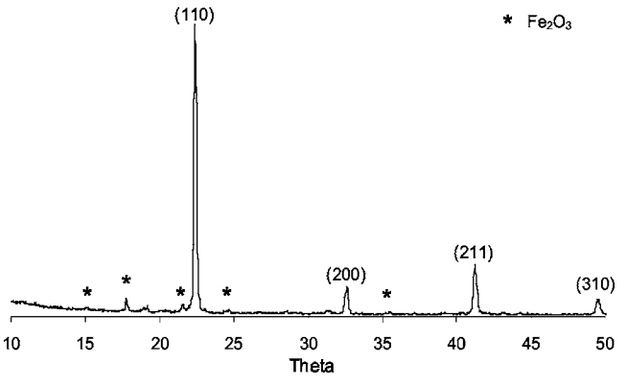

Figure 4. XRD diagram of iron thin film from $Fe(CO)_5$, at 673 K, overall flow rate 2320 sccm of N_2, $Fe(CO)_5$ mole fraction: 2.2×10^{-3} (run D12).

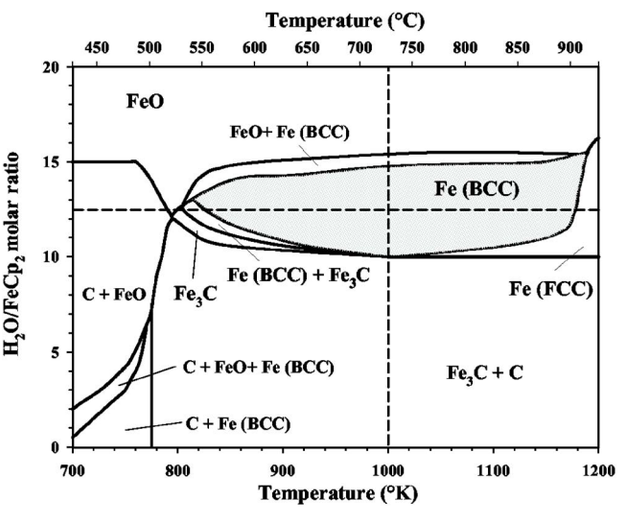

Figure 5. Theoretical phase diagram for the Fe-C-H-O system under 1 atm describing the film composition for various temperatures and $H_2O/FeCp_2$ molar ratios. Dotted lines correspond to the calculation conditions for the yield diagrams of Fig. 6.

Thermodynamic study.— For the thermodynamic calculations, a list was made of all the possible gaseous and condensed phases that can be formed from the combinations of the elements involved in the system, namely, C, Fe, H, and O. The total Gibbs energy of this system was minimized to obtain the number of molecules from each compound that form at various temperatures and $H_2O/FeCp_2$ molar ratios. The total Gibbs energy was minimized using the Gemini 2 software.[31] A set of 172 gaseous species and 14 condensed stoichiometric compounds were considered in the calculations. Their thermodynamic description was obtained from the SGTE (Scientific Group Thermodata Europe, Grenoble) data base. In composing the data base, the C-Fe metastable diagram was used, as established by Gustafson.[32] The use of this diagram allowed us to predict the amount of cementite that would be obtained in the film.

Figure 5 presents a deposition diagram calculated at 10^5 Pa as a function of deposition temperature and of the $H_2O/FeCp_2$ molar ratio in the input gas phase (95% Ar).

It reveals the possible existence of different domains composed of one, two, or three condensed phases. $H_2O/FeCp_2$ ratios lower than 10 yielded films with no contamination from carbon, but containing cementite above 773 K. $H_2O/FeCp_2$ ratios higher than approximately 14.5 yielded ferrous oxide, FeO. Between these two values, pure Fe is expected to be deposited. In these conditions, the cubic phase Fe bcc is expected in the films above 850 K; it is replaced by Fe fcc above 1160 K. Figure 6 presents two yield diagrams of the calculated number of moles of gaseous species as a function of the $H_2O/FeCp_2$ ratio in the input gas at 1000 K (left) and as a function of deposition temperature for an initial $H_2O/FeCp_2$ ratio of 12.5. These conditions correspond to the dotted lines shown in Fig. 6. Dashed domains in the two diagrams of Fig. 6 correspond roughly to conditions where pure Fe bcc is expected to be deposited. In these conditions, the reaction of $FeCp_2$ with water leads to a reductive atmosphere mainly composed of carbon monoxide and hydrogen. This overall reaction can be written as

$$4Fe(C_5H_5)_2 + 45H_2O \rightarrow 4Fe\ (BCC) + 35CO + 65H_2 + 5CO_2$$

As is often the case with thermodynamic calculations, these results should be considered as trends rather than precise predictions. However, they do indicate a window to obtain pure Fe with this system. The next sections confirm the useful trends of this calculation.

Influence of the growth conditions.— CVD runs were carried out at 973 K starting from a gas mixture of $FeCp_2$ and H_2O, but as the growth rate was relatively slow, the thickness was extremely weak after 20 min of reaction. Increasing the temperature to 1023 K gave layers with reasonable thicknesses. In situ observations re-

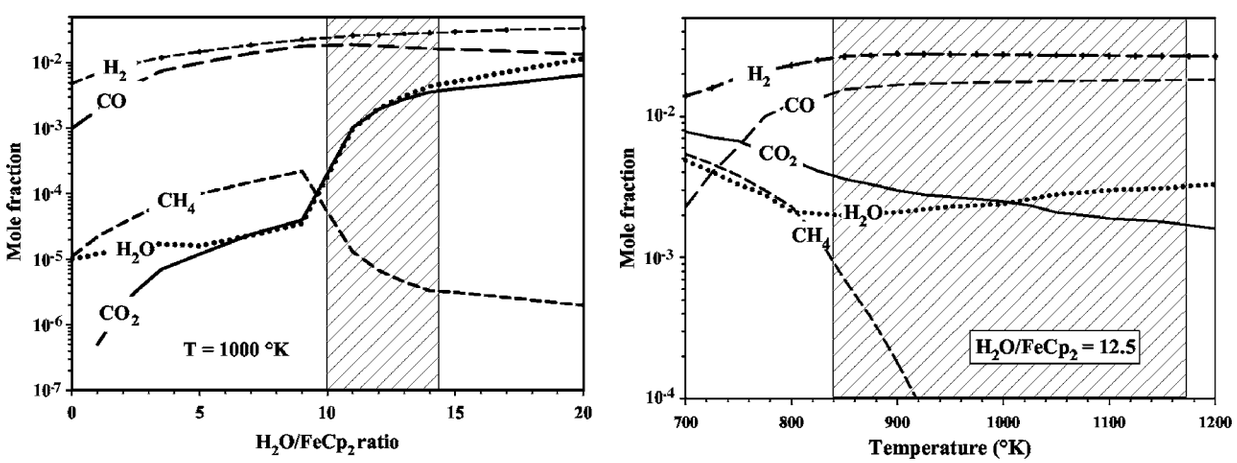

Figure 6. Calculated volumic fractions of gaseous species in the Fe-C-H-O system (Ar atmosphere). Species occurring at very low concentrations such as C_2H_4 and C_2H_2 are not plotted for clarity.

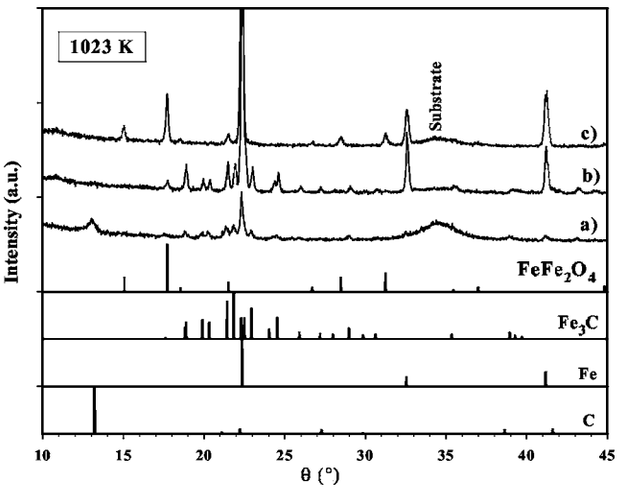

Figure 7. XRD grazing patterns (incidence angle 2°) of Fe layers grown by CVD on Si(111) at 1023 K for different $H_2O/FeCp_2$ molar ratios (deposition time = 15 min0: (a) $H_2O/FeCp_2$ = 0; (b) $H_2O/FeCp_2$ = 6; (c) $H_2O/FeCp_2$ = 8.

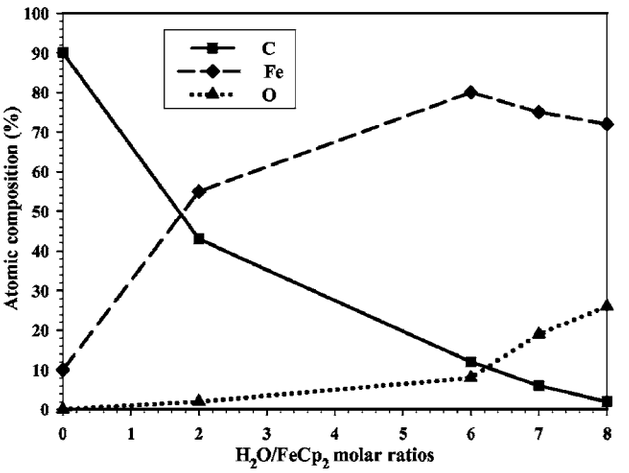

Figure 8. Atomic composition (EPMA) of iron layers deposited on Si(111) during CVD runs starting from different $H_2O/FeCp_2$ molar ratios (deposition time = 15 min).

vealed that during the first 10 min, a black powder layer was formed on Si substrates. After 10 min, a gray layer, apparently more compact and adherent, grew quickly over the whole sample, starting from the edges. This compact gray layer did not grow on the top of the black layer, but rather seemed to arise from the transformation of the initial powder layer. The samples became entirely gray after 15 min. On steel substrates, the formation of the gray layer started later (after 14–15 min) and the sample became entirely gray after 18–19 min. At 1073 K, an increase of the growth rate on Si(100) was observed. The formation of the gray layer started after only 5 min, compared to 12 min at 1023 K.This indicates that the increase in the temperature appreciably accelerated the formation of the compact gray layer.

Figure 7 shows the XRD diagrams of layers carried out at 1023 K starting from $FeCp_2$ and H_2O on Si(111) substrates. It confirms the tendencies anticipated by thermodynamic simulation, i.e., by increasing the water partial pressure, the amount of graphitic carbon in the film is lowered to negligible values, while levels of both iron and oxides rise. The layers are composed of C + Fe_3C + Fe for $H_2O/FeCp_2$ molar ratio = 0, Fe_3C + Fe + oxide traces for $H_2O/FeCp_2$ = 6, and Fe + Fe_3O_4 for $H_2O/FeCp_2$ = 8.

Electron-probe microanalysis (EPMA) confirmed the variation of Fe, C, and O composition with the $H_2O/FeCp_2$ molar ratios (Fig. 8). Thus, for a $H_2O/FeCp_2$ ratio = 0, the layers had a powdery appearance, being primarily made up of carbon and carbide. The increase of the $H_2O/FeCp_2$ ratio led to a fast reduction in the amount of carbon, a slight increase in oxygen, and a significant increase in iron. The highest Fe content was obtained for $H_2O/FeCp_2$ molar ratios in the range 4–6, which is why a series of experiments was carried out around these values. For $H_2O/FeCp_2$ molar ratios higher than 6, an increase in oxygen to the detriment of Fe was observed to the benefit of FeO and Fe_3O_4.

Analysis of the growth mode.— The XRD patterns show the presence of Fe (majority), Fe_3C, graphitic C, and oxides (FeO and Fe_3O_4) whose ratio changes with the deposition time. The formation of oxides is observed on Si(100) for $H_2O/FeCp_2$ molar ratios higher than 4. On steel, the formation of oxides starts for $H_2O/FeCp_2$ ratios higher than 6, maybe because a small part of the oxygen is consumed by oxidation of steel substrates. The deposition time seems to modify the nature and the structure of the layers (on Si and steel). For example, on Si, after 10 min, a significant quantity of graphitic carbon is incorporated into the layers and it decreases significantly by increasing the deposition time.

Assuming there is no preferential orientation, the relative intensity of the main diffraction lines suggests that the increase of the deposition time involves a decrease of the graphitic carbon content, which becomes practically undetectable after 20 min (Fig. 9). The formation of cementite was optimal after 15 min (during the formation of the gray layer), and then decreased with increasing deposition time. The amount of Fe_3O_4 remained almost constant, while the incorporation of FeO decreased after 12 min. On steel substrates, we observed the same tendencies as on Si.

The morphology and the microstructure of the layers depended significantly on the deposition time. Figure 10 shows SEM micrographs of Fe layers obtained starting from $FeCp_2$ and H_2O at 1023 K on Si(100) for different deposition times. A very porous layer composed of nanometric grains was observed after 10 min of deposition. It was black, powdery, and adhered poorly to the substrate. Increasing the deposition time led to an increase in grain size. After 12 min the grains started to grow, leading to the formation of

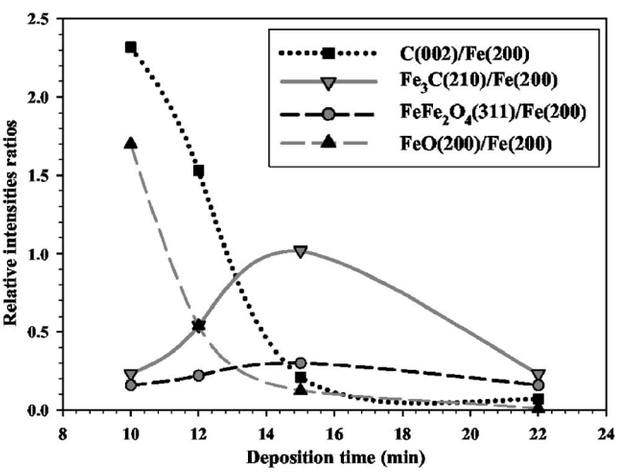

Figure 9. XRD relative intensities of C(002)/Fe(200), Fe_3C(210)/Fe(200), FeO(200)/Fe(200), and Fe_3O_4(311)/Fe(200) ratios of Fe layers grown on Si(100) at 1023 K for different deposition times, starting from $H_2O/FeCp_2$ molar ratio = 4.

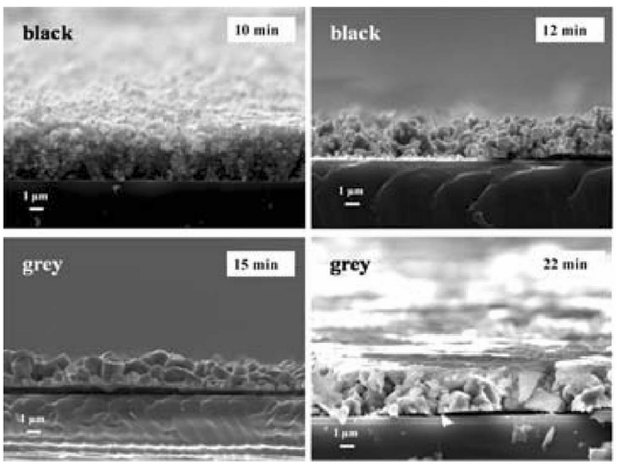

Figure 10. SEM micrographs of Fe layers obtained starting from $FeCp_2$ and H_2O at 1023 K on Si(100) for different deposition times ($H_2O/FeCp_2$ molar ratio = 4).

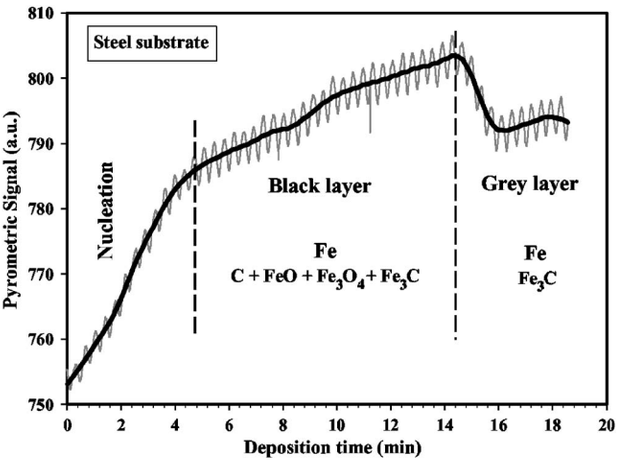

Figure 12. Variation of the pyrometric signal vs the deposition time of an Fe layer grown at 1023 K on steel substrate starting from $H_2O/FeCp_2$ molar ratio = 6 (the continuous line represents the smoothed pyrometric signal and the oscillations are due to the temperature control of the substrate).

the gray layer mentioned previously but exhibiting better adhesion to the substrate. After 20 min the layer becomes very compact and uniform and seems to be composed of equiaxial micrometric grains.

The morphological diversity of the Fe layers formed after the different durations of deposition made it difficult to determine the growth rate. Kinetic data were obtained by measuring the mass of deposited film on steel substrates for different deposition times (Fig. 11). For roughly 10 min, the mass of deposited film remained very low. This can be explained by the high porosity of the layer and by a significant deposition of graphitic C (light element) in the early stages of the growth during the formation of the powdery layer (Fig. 11 and 12). A steady state is observed after ca. 10 min with a constant growth rate of 0.156 mg min^{-1} cm^{-2} (ca. 12 μm/h), corresponding to the formation of the compact gray layer.

This growth mode was confirmed by in situ IR pyrometry analysis using a setup described elsewhere.[33] Details on this diagnostic tool for the control of CVD processes have recently been reported.[34] The pyrometric signal recorded during the CVD of Fe at 1023 K on steel starting from a gaseous $FeCp_2$-H_2O mixture is shown in Fig. 12.

Three main growth periods can be clearly distinguished. In the first period (0–4 min), the pyrometric signal strongly increases, likely due to a change of emissivity and of surface roughness corresponding to the nucleation step leading to the formation of the powdery black layer. During the second period, the deposition of C and oxides (FeO and Fe_3O_4), which both have higher emissivities than the substrate, explains the higher values of the pyrometric signal. As a result, the period between 5 and 14 min corresponds to the growth of the loose black layer. The third stage of growth appears after 14 min with an abrupt reduction of the pyrometric signal (occurring over only 1 min), before its stabilization to an approximately constant value. In the intermediate period, a decrease of C and Fe oxides in the layer was observed (Fig. 9). During this stage, the iron grains rapidly grow to uniformly cover the surface of the substrate forming the compact gray layer. Except for the nucleation step, the transition between the two growth modes is only of a few tens of seconds. Generally, the compact gray layer starts to be formed at one edge of the sample and the growth rapidly extends across the sample like a step-flow mechanism. Before the growth of the compact gray layer, the carbon is entirely consumed and the level of FeO decreases significantly, as shown in Fig. 9. These observations indicate reduction of the iron oxides by the C during the deposition of the powdery black layer. The growth of Fe layers at 1023 K is in good agreement with Ellingham's diagram. Once the codeposited C is consumed by the reduction of oxides, a metallic Fe film grows (bcc structure of the metal) with only slight contamination by Fe_3C.

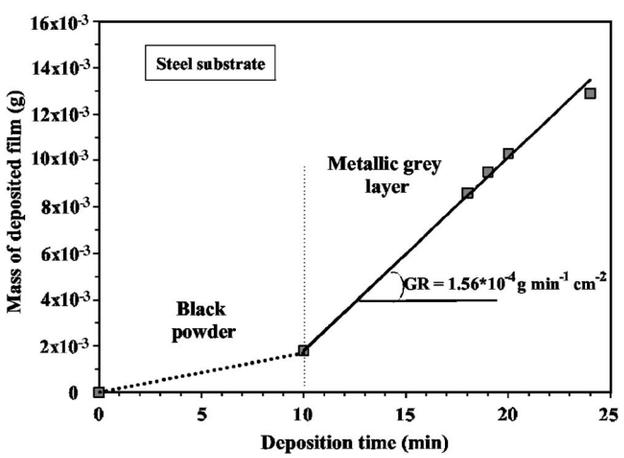

Figure 11. Variation of the film masses deposited on steel substrates for different deposition times at 1023 K ($H_2O/FeCp_2$ ratio = 6).

Conclusion

Relatively pure thin layers of iron were obtained, with high growth rates, by atmospheric pressure MOCVD, either from $Fe(CO)_5$ in the temperature range 473–773 K, or $FeCp_2$ and H_2O in the temperature range 973–1023 K.

$Fe(CO)_5$ is a satisfactory precursor for iron thin-film deposition under atmospheric pressure, even without additives in the gas phase. With this precursor, the growth rate is closely related to gas velocity as a short residence time in the deposition zone lowers the formation of byproducts, which penalize the layer growth. Nevertheless, without additive in the gas phase, an increase of the precursor mole fraction favors the incorporation of carbon into the film. As a result, the window for the growth parameters is relatively narrow so it will be certainly hard to optimize the use of $Fe(CO)_5$ in a large-scale reactor process, due to its sensitivity to the variation of the local conditions.

The use of $FeCp_2$ alone leads to a pulverulent and nonadhesive deposit, but the addition of water vapor to the gas phase leads to the formation of relatively pure Fe thin layers. The layers are essentially composed of Fe, but also contain secondary phases like Fe_3C, FeO,

Fe_3O_4, and C, the proportion of which depends on the CVD conditions. The morphology and the structure of the layers change with the deposition time. In addition to nucleation, growth occurs in two steps: (*i*) the initial formation of a black porous layer that (*ii*) densifies in a few minutes as a result of grain growth and coalescences for increasing deposition times leading to compact gray metallic films. This two-step mechanism was confirmed by kinetics studies and by in situ IR pyrometric diagnostic. XRD and EPMA analyses show that the highest purity of the Fe layers is obtained for $H_2O/FeCp_2$ ratios between 4 and 6. The experimental results are in fairly good agreement with the thermodynamic model made of the Fe-C-H-O system under atmospheric pressure.

National Center for Scientific Research assisted in meeting the publication costs of this article.

References

1. G. J. M. Dormans, *J. Cryst. Growth*, **180**, 806 (1991).
2. G. T. Stauf, D. C. Dristcoll, P. A. Dowben, S. Barfuss, and M. Grade, *Thin Solid Films*, **153**, 421 (1987).
3. R. Kaplan and N. Bottka, *Appl. Phys. Lett.*, **41**, 972 (1982).
4. P. J. Walsh and N. Bottka, *J. Electrochem. Soc.*, **131**, 444 (1984).
5. P. A. Lane, P. J. Wright, P. E. Oliver, C. L. Reeves, A. D. Pitt, J. M. Keen, M. C. L. Ward, M. E. G. Tisley, N. A. Smith, B. Cockayne, and I. Rex Harris, *Chem. Vap. Deposition*, **3**, 97 (1997).
6. P. A. Lane and P. J. Wright, *J. Cryst. Growth*, **204**, 298 (1999).
7. H. J. Haugan, B. D. McCombe, and P. G. Mattocks, *J. Magn. Magn. Mater.*, **247**, 296 (2002).
8. R. Feurer, M. Larhafi, R. Morancho, and R. Calsou, *Thin Solid Films*, **167**, 195 (1988).
9. D. V. Baxter, M. H. Chisholm, G. J. Gama, A. L. Hector, and I. P. Parking, *Chem. Vap. Deposition*, **1**, 49 (1995).
10. W. Luithardt and C. Benndorf, *Thin Solid Films*, **290/291**, 200 (1996).
11. J. A. Long, V. G. Riggs, A. T. Macrander, and J. W. D. Johnston, *J. Cryst. Growth*, **77**, 42 (1986).
12. D. L. S. Brown, J. A. Connor, M. L. Leung, M. I. Paz-Andrade, and H. A. Skinner, *J. Organomet. Chem.*, **110**, 79 (1976).
13. I. B. Johns, E. A. McElhil, and J. O. Smith, *J. Chem. Eng. Data*, **7**, 277 (1962).
14. F. B. McCormick, W. L. Gladfelter, and Y. Senzaki, U.S. Pat. 5,314,727 (1994).
15. F. B. McCormick, W. L. Gladfelter, and Y. Senzaki, U.S. Pat. 5,372,849 (1994)
16. J. Kane and H. Schweizer, U.S. Pat. 3,914,515 (1975).
17. M. Mukaida, I. Hiyama, T. Tsunoda, and Y. Imai, *Thin Solid Films*, **381**, 214 (2001).
18. A. Erbil, U.S. Pat. 4,927,670 (1990).
19. H. Torii, E. Fujii, M. Aoki, and K. Ochiai, U.S. Pat. 4,975,324 (1990).
20. E. Fujii, H. Torii, A. Tomozawa, R. Takayama, and T. Hirao, *J. Cryst. Growth*, **151**, 134 (1995).
21. H. Choi, U.S. Pat. 6,777,565 (2004).
22. G. T. Stauf, D. C. Dristcoll, P. A. Dowben, S. Barfuss, and M. Grade, *Thin Solid Films*, **153**, 421 (1987).
23. G. J. M. Dormans, *J. Cryst. Growth*, **108**, 806 (1991).
24. F.-D. Duminica, F. Maury, and F. Senocq, *Récents Progrès en Génie des Procédés*, Vol. 92, L2/1-8, Lavoisier, Paris (2005).
25. K. Elihn, F. Otten, M. Boman, F. E. Kruis, H. Fissan, and J.-O. Carlsson, *Nanostruct. Mater.*, **12**, 79 (1999).
26. F. Otten, K. Elihn, F. E. Kruis, M. Boman, J.-O. Carlsson, and H. Fissan, *J. Aerosol Sci.*, **29**, 125 (1998).
27. F. Maury, *Chem. Vap. Deposition*, **2**, 113 (1996).
28. T. Delsol, F. Maury, and F. Senocq, in *Proceedings of the 15th European Conference on Chemical Vapor Deposition*, R. Fischer, Editor, PV 2005–09, p. 638, The Electrochemical Society Proceedings, Pennington, NJ (2005).
29. F. D. Duminica, F. Maury, C. Vahlas, F. Senocq, and T. Delsol, in *Proceedings of the 15th European Conference on Chemical Vapor Deposition*, R. Fischer, Editor, PV 2005-09, pp. 644, The Electrochemical Society Proceedings, Pennington, NJ (2005).
30. F. Fau-Canillac and F. Maury, *Surf. Coat. Technol.*, **64**, 21 (1994).
31. http://thermodata.online.fr/thermafr/france.html
32. P. Gustafson, *Scand. J. Metall.*, **14**, 259 (1985).
33. C. Gasqueres, F. Maury, and F. Ossola, *Chem. Vap. Deposition*, **9**, 34 (2003).
34. C. Gasqueres, F. D. Duminica, and F. Maury, *Chem. Eng. Proc.*, Submitted.